

An Advanced Method for Deriving Latent Energy Flux from a Scanning Raman Lidar

D. I. Cooper,* W. E. Eichinger, J. Archuleta, L. Hipps, C. M. U. Neale, and J. H. Prueger

ABSTRACT

One of the fundamental issues with lidar-derived evapotranspiration estimates is its reliance on tower-based measurements of Monin–Obukhov similarity variables, specifically the Obukhov length (L) and the friction velocity (u_*). Our study indicates that L can be derived in the atmospheric surface layer directly from lidar range-height scans by estimating the integral length scale (ILS). Data from both three-dimensional sonic anemometers mounted on towers and lidar data collected during two subsequent field experiments were analyzed using autocorrelation analysis to estimate the ILS. The ILS values were then transformed into L values using a power-law similarity model and were compared to coincident tower-based observations. The comparisons between tower-based eddy covariance sensors and lidar data show that the lidar-derived L values are within the expected uncertainty and variability of standard point sensor measured observations. An additional model for estimating the friction velocity from the Obukhov length was also derived, and both L and u_* were used to calculate the latent energy flux from lidar without external measurements. The evapotranspiration fluxes from the standard method and the new advanced method were compared with eddy covariance fluxes, and it was found that the advanced method is superior.

THE rate and distribution of water use in the landscape (evapotranspiration) is a fundamental parameter that agronomic and watershed managers require when attempting to optimize hydrological resources. Evapotranspiration (ET) couples the soil–water–plant system to the atmosphere and is therefore a spatially dependent variable. Up to now, however, the measurement of ET has been made almost exclusively by point sensors that average this parameter across time and space. Scanning Raman water vapor lidars have been used to map the water vapor scalar and flux over various surfaces for the past decade (Cooper et al., 1992; Eichinger et al., 2006). The utility of the scanning Raman lidar to derive maps of ET (latent energy) flux has been dependent on turbulence parameters measured independently from tower-based three-dimensional sonic anemometers for critical variables including the Obukhov length, L , and the friction velocity, u_* (Cooper et al., 2000).

The Obukhov length is used to adjust flux estimates for stability in the first few meters of the of the atmosphere directly above the crop surface, and u_* is the

primary variable of the momentum flux that exchanges water vapor between the surface and the atmosphere (Eichinger et al., 2000). Currently, micrometeorological theory and technique incorrectly assume that L and u_* measurements from point sensors can be applied uniformly over an entire crop surface to estimate ET for a given spatial region. The use of lidar to infer the spatial variability of ET has been limited due to the requirement that sonic anemometers be collocated with the lidar. Furthermore, the appropriate density of tower-based observations for spatial variability studies is unknown, thus it is attractive to explore ways to advance techniques where lidar can be used to roughly estimate L and u_* independent of point sensors for ET flux mapping. Our hypothesis is that it should be possible to estimate L and u_* from lidar data without the use of ancillary tower measurements by calculating the integral length scale (Wilson et al., 1981). In addition, the method described here could be applied to other types of lidars and offers the opportunity to spatially resolve L and u_* , which would improve our understanding of surface–atmosphere exchange processes.

Fundamental work by Wilson et al. (1981) suggested that L is related to simple statistical properties of passive scalars in the atmosphere, such as the integral time scale (ITS) and, by extension, the integral length scale (ILS). The ILS is the radial distance that energy and mass in the atmosphere are transported downwind by large coherent eddies (Tennekes and Lumley, 1972) and is the spatial analog of the ITS. Large eddies are those that are greater than the ILS and, conversely, small eddies are equal to or less than the ILS (Frisch, 1995). The ILS is computed here using a purely statistical property of the spatial data, the autocorrelation function of space–concentration transects extracted from lidar-measured range-height scans. To compute the ILS, the autocorrelation function is calculated and then the function is integrated. Once the autocorrelation-derived ILS is estimated, a similarity function is used to relate the ILS to L , and then a second model relates L to u_* , thus creating spatially resolved turbulence parameters. Obtaining L and u_* values in this way allows estimates of the water vapor flux from the lidar with little dependency on external point sensors for turbulence and stability parameters.

LIDAR

The Los Alamos National Laboratory's Raman lidar generated volume images from two-dimensional range-height scans of water vapor. Details on the method and

D.I. Cooper and J. Archuleta, Los Alamos National Lab., MS J577, Los Alamos, NM 87545; W.E. Eichinger, Iowa Inst. for Hydraulic Research, Univ. of Iowa, Iowa City, IA 52242; L. Hipps, Dep. of Plants, Soils and Biometeorology, Utah State Univ., Logan UT 84322; C.M.U. Neale, Dep. of Biological and Irrigation Engineering, Utah State Univ., Logan UT 84322; and J.H. Prueger, USDA National Soil Tilth Lab., Ames IA 50011. Received 15 Apr. 2005. *Corresponding author (dcooper@lanl.gov).

Published in *Agron. J.* 99:272–284 (2007).

Special Submissions

doi:10.2134/agronj2005.0110s

© American Society of Agronomy

677 S. Segoe Rd., Madison, WI 53711 USA

Abbreviations: ABL, atmospheric boundary layer; ET, evapotranspiration; ILS, integral length scale; ISSA, integral scale similarity approach; ITS, integral time scale; MISA, micrometeorological integrated similarity approach; SMEX, Soil Moisture Experiment.

operation of the scanning lidar are described in Eichinger et al. (1999). The radial range of the lidar extended to >500 m, with a spatial resolution of 1.5 m. The azimuthal scanning range covered up to 180° in 10° azimuthal increments, while the elevation scanning range was ±6° from horizontal in 0.25° elevation increments. Each range-height scan required no more than 43 s to complete with a set of 24 line-of-sight scans, requiring about 15 min to complete a full set of range-height scans across the 180° swath. The vertical scans acquired lines of sight from below the canopy up to 50 m into the lower atmospheric boundary layer (ABL). From the two Bosque field experiments, 122 data sets of scans were selected for further processing because they represent coincident observations with the eddy covariance sensors. Furthermore, the periods were convective and unstable, the wind was from a direction with ample fetch so that the region sampled is considered homogeneous and advection was minimal, and the periods were during storm-free, clear-sky conditions.

The absolute accuracy of the lidar was shown to be ±0.0034 kg kg⁻¹ at the 95% confidence level; differential precision is on the order of 0.0001 kg kg⁻¹ (Cooper et al. 1996; Eichinger et al., 1994). While the lidar scanning rate is modest, it does provide an opportunity to evaluate some aspects of the turbulent exchange process. Horizontal transects parallel to the top of the canopy were extracted from these vertical range-height scans by averaging portions of several lines of sight (4–6) together for the region of interest (Fig. 1), thereby ensuring extensive spatial data.

OBUKHOV THEORY

To estimate a flux with the lidar, a Monin–Obukhov similarity model is used, which uses L to correct the model profile of moisture for stability and u_* is the transport and exchange term. The latent energy flux (LE) estimates are obtained from lidar-measured profiles of water vapor mixing ratio with height using a similarity model (Brutsaert, 1982):

$$q(z) = - \frac{LE}{l_e k u_* \rho} \left[\ln(z) - \psi_v \left(\frac{z}{L} \right) \right] + \left[q_s - \frac{LE}{l_e k u_* \rho} \ln(z_0) \right] \quad [1]$$

where $q(z)$ is the water vapor mixing ratio at height z (kg kg⁻¹), l_e is the latent heat of vaporization (J kg⁻¹), k is the von Karman constant, ρ is the air density (kg m⁻³), ψ_v is the stability correction factor for water vapor, q_s is water vapor at the surface, and z_0 is the surface roughness (m) (see Appendix).

Equation [1] assumes that LE is constant with height, and thus this model is appropriate for the “constant flux layer” several meters above the surface. The profiles of water vapor allow a least squares determination of the slope of the profile, $LE/(l_e k u_* \rho)$. The method requires a value of L to determine the slope of the profiles and a

value of u_* to obtain the evapotranspiration rate, LE, from the slope of the water vapor profile. The profile is constructed with spatially resolved water vapor concentrations from a 50- to 75-m² region, depending on footprint requirements (Cooper et al., 2003).

The Monin–Obukhov length (L) is the central micrometeorological variable in similarity-based turbulence parameterization used to describe the degree of atmospheric stability (Monin and Yaglom, 1971), which can be thought of as the height at which mechanical and buoyancy forces are approximately equal (by convention, when $L < 0$, the atmosphere is considered unstable, and when $L > 0$, the atmosphere is stable) and calculated as the ratio of surface layer shear forces to those due to buoyancy (Stull, 1988). The value of L is given by

$$L = - \frac{\rho u_*^3}{kg \left(\frac{w' \theta_v'}{\theta_v c_p} \right)} \quad [2]$$

where g is the acceleration due to gravity (m s⁻²), $\overline{w' \theta_v'}$ is the time-averaged virtual sensible heat flux (J m⁻² s⁻¹), θ_v is the virtual temperature (K), and c_p is the specific heat of air (J kg⁻¹ K⁻¹).

Specific details on the now-standard approach to the derivation, computation, and validation of the lidar-derived latent energy fluxes can be found in Eichinger et al. (2000). By measuring the spatially resolved water vapor gradient and deriving L and u_* from lidar data alone, the critical parameters for estimating the latent energy flux (Eq. [1]) would be available independent of tower-based observations.

METHODOLOGY

The Obukhov length and the characteristic length scale of turbulent transport appear to be related (Wilson et al., 1981) and are typically derived from tower-based sensors collecting time-series data. The characteristic length scale is derived from the characteristic time scale with the inclusion of a friction velocity transport estimate. The deviations from the mean of passive scalars in time or space is thought to represent the passing of a turbulent event. When evaluating a time series and using one of the many analysis methods such as eddy covariance, spectral, etc., information about the fate and behavior of these structures involved in mass and energy exchange can be derived. In contrast to time-series analysis of atmospheric turbulence, spatial-series studies are relatively rare in the literature. Direct spatial measurements of turbulent length scales have been made using aircraft observations in at least two experiments involving scalars and wind in the marine boundary layer, where the convective structures are somewhat homogeneous (Durand et al., 2000; Lenschow and Stankov, 1986). The use of aircraft in the ABL, however, is restricted by the inability to acquire data close to the ground (Mahrt, 1998). In contrast to the aircraft approach, multidimensional lidar data offer the ability to directly observe some of the spatial properties of tur-

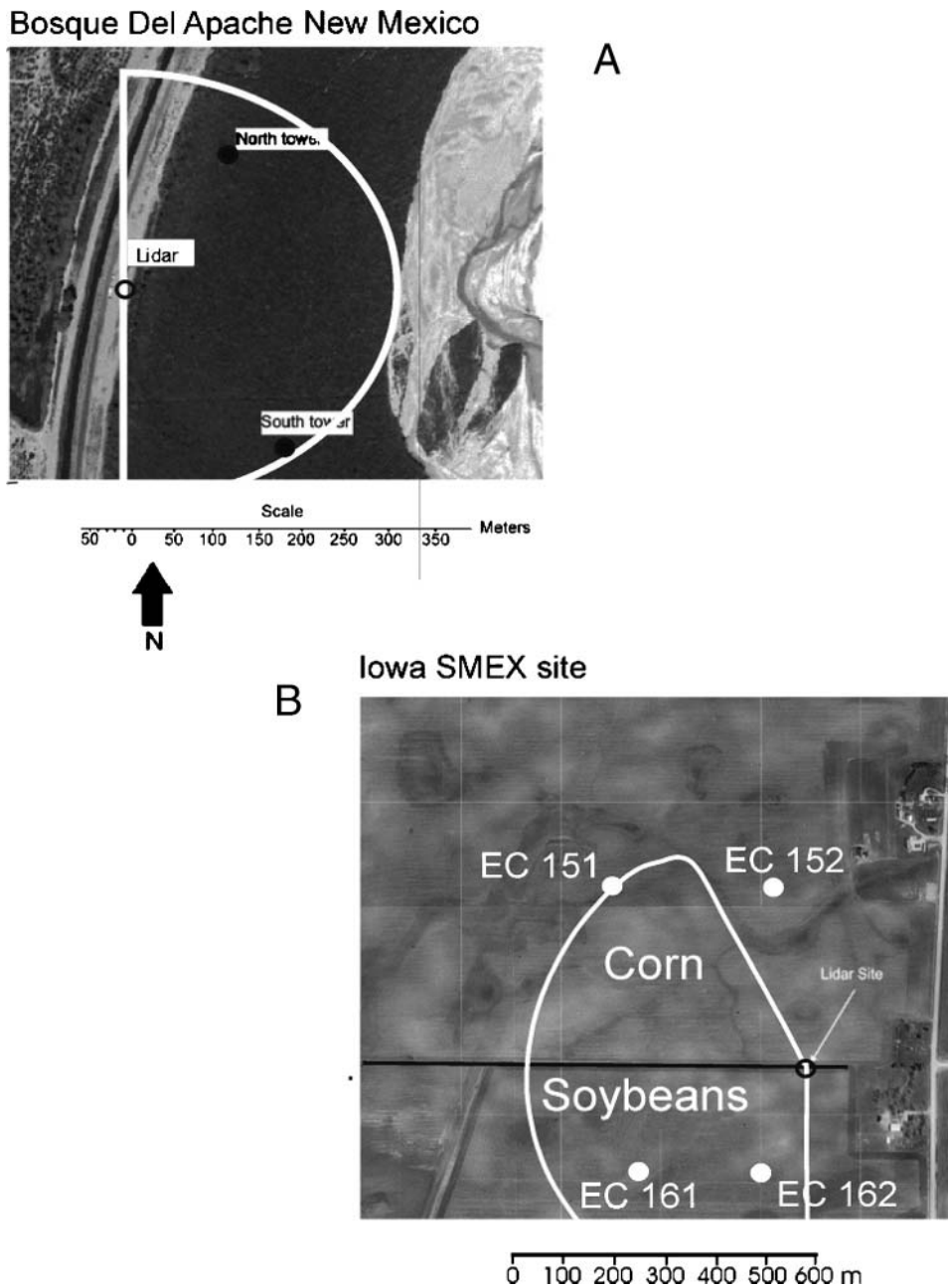


Fig. 1. (A) Site map showing the location of the Bosque relative to the state of New Mexico, and (B) an infrared aerial photograph of the Bosque indicating the location of the lidar and the lidar scanning pattern used to generate horizontal spatial series.

bulent features evolving between the surface and the first tens of meters of the ABL, and thus offer an additional and arguably improved view of the surface-atmosphere exchange process.

The ILS is derivable from both temporal and spatial series and is used here to determine the characteristic time or space in which turbulent events remain coherent. The ILS is estimated by integrating a given variable's autocorrelation function. Using a similarity model, the ILS is transformed into L values. Our fundamental assumption is that a scalar spatial series, derived from the lidar at a fixed height parallel to the surface, will contain within its variations turbulence properties

similar to those seen in the more traditional time-series measurements such as fast-response hygrometers.

Integral Scales from Autocorrelation

Integral time and length scales were estimated from moisture observations with both tower-based hygrometer time series and lidar remotely sensed spatial series. The ILS (Λ) is usually derived from the ITS (τ) by using a transport term, $\Lambda = \bar{u}\tau$, where \bar{u} is the mean downwind component (Tennekes and Lumley, 1972). Because lidar data is inherently spatial, the mean wind is not required, allowing the spatial scale to be computed directly from τ

as the integral of the autocorrelation function of the water vapor, integrated to infinity (Kaimal and Finnigan, 1994; Pope, 1998). Thus, the integral length scale for water vapor (Λ_q) is

$$\Lambda_q = \int_0^{\infty} \rho_q(\xi) d\xi \quad [3]$$

where ρ_q is the water vapor density (kg m^{-3}) and ξ is the lag in space or time (m or s). The autocorrelation function for water vapor is

$$\rho_q(\xi) = \frac{\overline{q_i' q_{i+\xi}'}}{\sigma_q^2} \quad [4]$$

where q_i is an instantaneous observation of water vapor at some time (for hygrometer data) and σ_q^2 is the variance of q (water vapor) from a temporal or spatial series. The conditional water vapor estimates are

$$\begin{aligned} q_i' &= q_i - \bar{q} \\ q_{i+\xi}' &= q_{i+\xi} - \bar{q} \end{aligned} \quad [5]$$

The integration of autocorrelation functions for water vapor across infinite spatial lags is not possible, and it is assumed here for convenience that the finite sampled population is adequate. Instead, the lag length (or time) of the first zero crossing of the autocorrelation function (ξ_{ρ_0}) is chosen as the integrating limit (Kaimal and Finnigan, 1994). Further, there is a temporal (t) and spatial (S) data constraint for estimating the ILS or ITS such that $t \gg \tau$ (Garratt, 1992) and by extension, $S \gg \Lambda$. In practice, the equation defining Λ from lidar spatial data is:

$$\Lambda_{q \text{ lidar}} = \int_0^{\xi_{\rho_0}} \rho_q(\xi) d\xi \quad [6]$$

where $\Lambda_{q \text{ lidar}}$ is the integral length scale derived from lidar data. Autocorrelation functions for water vapor observed by both the lidar and krypton hygrometer were calculated for the unstable case. To illustrate the sequence of processing steps used to compute the ILS, an example lidar data set is shown from the raw spatial series to the autocorrelation plot (Fig. 2A–2D). Lidar range-resolved transects of water vapor concentration 300 m long, starting 100 m from the lidar and extending 400 m away, were extracted from several horizontal lines of sight averaged together at the mean height of 2.7 m above the canopy, coincident with the tower-based sensors (Fig. 2A). The spatial series is first normalized by detrending the data using a least squares linear fit (Fig. 2B), and then a low-pass filter is applied to smooth the high frequency components. The data were smoothed with a Savitzky–Golay technique (Fig. 2C; Press et al., 1989). The normalized and smoothed data were then used to compute the autocorrelation (Eq. [2]) and the resulting functions were then integrated up to the first zero crossing (Fig. 2D).

Estimating the Obukhov Length

Wilson et al. (1981) showed that for non-neutral atmospheres, the eddy diffusivity could be calculated from the integral time scale:

$$K = \sigma_w^2 \tau_q \quad [7]$$

where K is the eddy diffusivity ($\text{m}^2 \text{s}^{-1}$) and σ_w^2 is the variance in the vertical wind (m s^{-1}). In particular, for a passive scalar such as water vapor, the diffusivity could be related to L and the friction velocity u_* as

$$K = \frac{ku_*(z-d)}{\phi_w\left(\frac{z}{L}\right)} \quad [8]$$

where d is the displacement height (m) and ϕ_w is the profile function for momentum. It can be seen from Eq. [7] and [8] that the diffusivity is a function of L or the ITS.

The ITS (τ) is estimated from point sensor data, typically as a function of the roughness element length, such as the height of the canopy above ground, h , or $(z-d)$ and the transport velocity or variance such as u_* , σ_u , σ_v , or σ_w (Baldocchi 1997, Blackadar 1997). Both studies used parameterizations for τ using the height of the canopy:

$$\tau = \frac{0.17h}{\sigma_w} \quad [9]$$

Under near-neutral conditions, Raupach (1989) suggested that τ could be based on a scaled height and the velocity variance:

$$\tau = \frac{k(z-d)}{\sigma_w} \quad [10]$$

Monin and Yaglom (1971) showed that the ratio of the velocity variance to the friction velocity is proportional to a set of universal similarity functions and can be estimated by a similarity function incorporating both the Obukhov length and the friction velocity (Panofsky and Dutton, 1984):

$$\sigma_w = 1.25u_* \left(1 - \beta_1 \frac{z}{L}\right)^a \quad [11]$$

where β_1 is nominally 3 and a is 1/3. By substituting Eq. [11] into Eq. [10], a stability-corrected similarity-based ITS is estimated:

$$\tau = \frac{k(z-d)}{1.25u_* \left(1 - \beta_1 \frac{z}{L}\right)^a} \quad [12]$$

By multiplying Eq. [11] by the mean wind, an ILS (Λ) is estimated as

$$\Lambda = \bar{u} \left[\frac{k(z-d)}{1.25u_* \left(1 - \beta_1 \frac{z}{L}\right)^a} \right] \quad [13]$$

Equation [13] can be simplified in terms of the number of required variables by noting that

$$\bar{u}(z) = \frac{u_*}{k} \left[\ln\left(\frac{z}{z_0}\right) - \psi_m\left(\frac{z}{L}\right) \right] \quad [14]$$

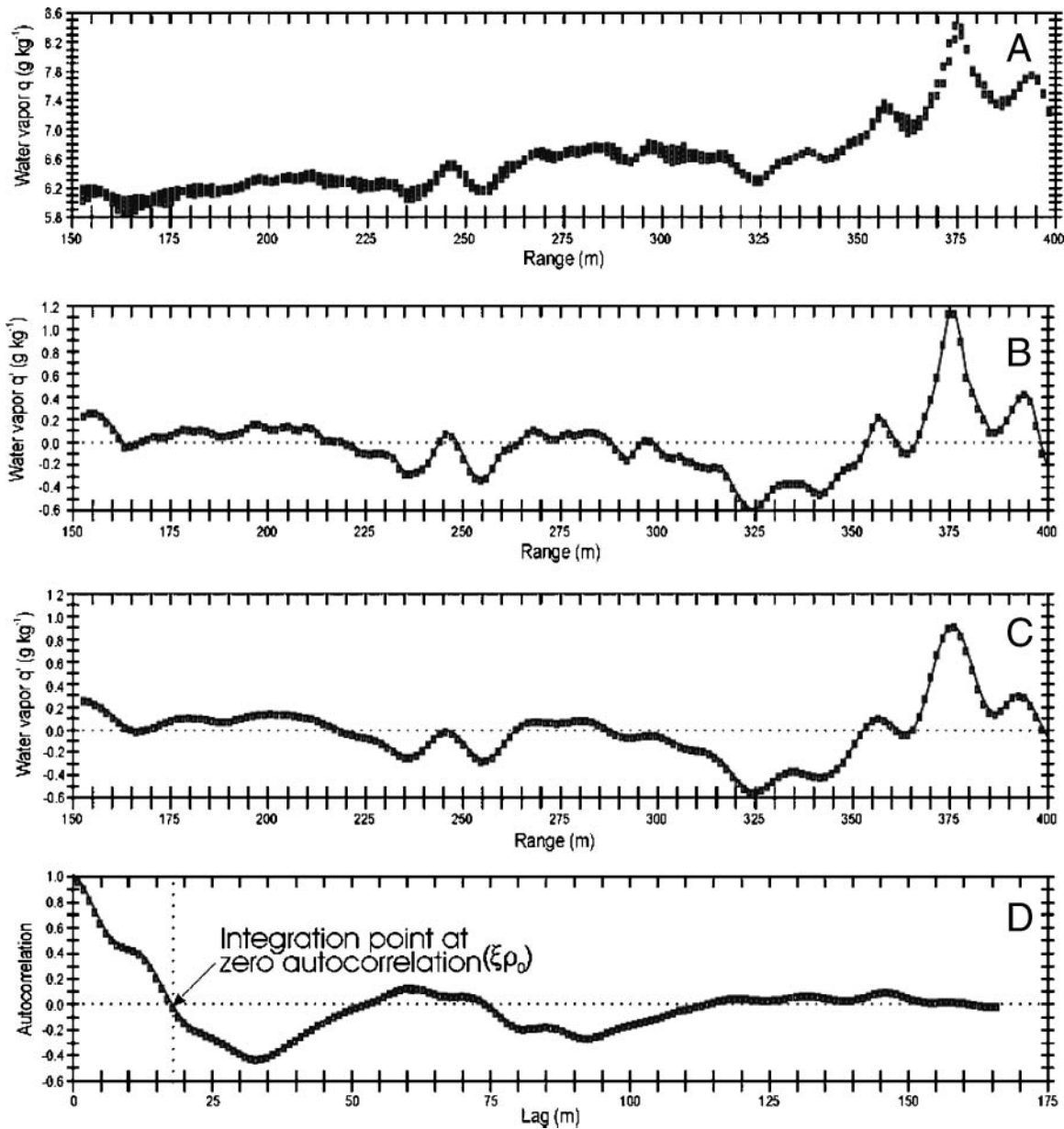


Fig. 2. The processing of a horizontal spatial series from 9 Sept. 1998 at 1208 h illustrating: (A) “raw data,” (B) conditional water vapor mixing ratio (q) series, (C) smoothed conditional data, and (D) autocorrelation function for the spatial series. ξ_{ρ_0} is the first zero crossing of the autocorrelation function.

so that by the substitution of Eq. [14] into Eq. [13], u_* also conveniently drops out:

$$\Lambda = [\ln(z/z_0) - \psi_m(z/L)] \frac{z-d}{1.25\{1 - [\beta_1(z-d)/L]^a\}} \quad [15]$$

This equation can be algebraically solved for L , with the following result:

$$L = \frac{(z-d)\beta_1}{1 - \left(\frac{\Lambda_{q \text{ lidar}}}{C_1(z-d)\{\ln[(z-d)/z_0] - \psi_m[(z-d)/L]\}} \right)^a} \quad [16]$$

where $\Lambda_{q \text{ lidar}}$ is derived from lidar data and C_1 , a height-adjusted profile fitting constant, has been substituted for the empirically derived constant of 1.25 in Eq. [12] thru [15]. As used here, C_1 is also an empirically derived function to relate canopy-measurement height geometries across a modest range of values instead of the standard 1.25 (Panofsky and Dutton, 1984). The value of 1.25 was initially derived from a limited set of experimental observations for “large z/L values” (Merry and Panofsky, 1976, Panofsky et al., 1977). We added an empirical height adjustment factor to account for differing canopy and measurement heights: $C_1 = 1.25 + [1.5/\ln(z/z_0)]$ for various combinations of instrument and canopy height and range between 0.1 and 2. The stability

correction function for momentum, ψ_m , in unstable atmospheric conditions is given by

$$\begin{aligned} \psi_m\left(\frac{z-d}{L}\right) &= 2 \ln\left(\frac{1+x}{2}\right) + \ln\left(\frac{1+x^2}{2}\right) \\ &\quad - 2 \arctan(x) + \frac{\pi}{2} \\ x &= \left(1 - 16\frac{z-d}{L}\right)^{1/4} \end{aligned} \quad [17]$$

Equation [16] requires only knowledge of the ILS to determine L , albeit by an iterative process since ψ is an asymptotic function of L . From Eq. [16], lidar data can be used to directly estimate L without tower-based wind sensor data through the computation of the ILS.

Estimating the Friction Velocity From Lidar Data

A further extension of the autocorrelation-derived ILS uses similarity theory to estimate the friction velocity (u_*) from the Obukhov length (L). The u_* variable is the critical transport term in the Monin–Obukhov flux parameterization used to estimate ET (Eq. [2]) from the lidar. The derivation of u_* is as follows, by reiterating Eq. [12]:

$$\tau = \frac{k(z-d)}{1.25u_*\left(1 - \beta_1\frac{z-d}{L}\right)^a} \quad [18]$$

and solving for u_* , the equation now is

$$u_* = \frac{k(z-d)}{\tau 1.25\left(1 - \beta_1\frac{z-d}{L}\right)^a} \quad [19]$$

Further, Wilson et al. (1981) showed that τ is related to L by

$$\tau = 0.5(z-d)\left(1 - \beta_2\frac{z-d}{L}\right)^b \quad [20]$$

then, by substitution of τ with Eq. [19], u_* is estimated as a function of L :

$$u_* = \left[\frac{k(z-d)}{C_1\left(1 - \beta_1\frac{z-d}{L}\right)^a} \right] \left[0.5(z-d)\left(1 - \beta_2\frac{z-d}{L}\right)^b \right]^{-1} \quad [21]$$

with β_1 and β_2 equal to 3 and 6, respectively, and a and b equal to 1/3 and 1/4, respectively (Stull, 1988). In Eq. [21], C_1 is substituted for the constant 1.25 in Eq. [19].

EXPERIMENTAL OVERVIEW

The data used in this study were obtained from two separate sites on three different dates, the first site being a salt cedar (*Tamarisk* spp.) riparian zone in the southwest USA on the Rio Grande River (Bosque experiment) where the model relationships were developed (Cooper et al., 2003) and the second site, where the method was tested, was over adjacent corn (*Zea mays* L.) and soybean [*Glycine max* (L.) Merr.] fields in Iowa during the Soil Moisture Experiment (SMEX; Kustas et al., 2003; Table 1). The riparian zone was located adjacent to the Rio Grande River at the Bosque Del Apache Wildlife Refuge in the semiarid south-central part of New Mexico. The agricultural site was located in the temperate climate of south-central Iowa.

Bosque

The vegetation at the Bosque consisted almost entirely of uniformly dense riparian salt cedar. During the 1999 study period, the salt cedars were actively growing leaves and standing in several inches of water, while in 1998 the growing season was near its end, and the soil was relatively dry. Winds were generally mild, at $<2 \text{ m s}^{-1}$ during both periods, typically northerly in the early morning and periodically reversing direction by midmorning to become southerly. Since the study site was located on a floodplain, the surface topography underneath the salt cedars was relatively flat. The spatial extent of the vegetation in the riparian corridor varied in width between 300 and 700 m and extended both north and south for several kilometers; thus, as long as the winds were from the southern or northern directions, the fetch at the site was several kilometers long. Data obtained during rainy periods or during westerly advective wind conditions were excluded from the analysis.

Soil Moisture Experiment

The vegetation at the Iowa SMEX site consisted of a corn field and an adjacent soybean field. The corn was rapidly maturing while the soybean was still fairly small and young, thus creating an environment with a tall closed canopy (corn) and a short, open, soil–canopy condition (soybean; Table 1). Winds were generally at 4.5 m s^{-1} at 255° . The surface topography had almost no slope, with crop rows running east–west. Both the corn and soybean fields were in excess of 1 km in length and width. Data from periods when rain occurred were not used in this study.

Table 1. Experimental sites, locations, dates, surface cover, leaf area index (LAI), canopy heights and canopy closure, and instrument heights.

Experiment	Location	Date	Surface	LAI	Canopy height	Instrument height
					m	
Bosque 1998	34°N, 107°W	Sept. 1998	salt cedar	2	5, closed	7.7
Bosque 1999	34°N, 107°W	June 1999	salt cedar	1.5	5, closed	7.7
SMEX	41°N, 93°W	July 2002	corn	3.4	1.4, closed	3.9
SMEX	41°N, 93°W	July 2002	soybean	1.9	0.34, open	1.9

Micrometeorological Instruments

In the Bosque, two 12-m-tall micrometeorological towers were positioned between the western edge of the salt cedars and the Rio Grande, at a distance of about 300 m from the river. The two towers were separated from each other by 585 m in the north-south direction. At the Iowa site, four 5-m towers were positioned in the corn (two) and soybean (two) fields. The heights of the instruments and the vegetation are given in Table 1. The towers were instrumented with CSAT-7 three-axis sonic anemometers (Campbell Scientific, 1998), fine wire thermocouples, fast-response hygrometers (KH2O krypton [Campbell Scientific, Logan, UT] or LI-COR 7500 [LI-COR, Lincoln, NE]), and Vaisala HMP45a temperature-humidity probes (Vaisala, Helsinki, Finland). Leaf area index (LAI) was measured by a Licor 2000 radiative LAI meter. Turbulent fluxes of sensible heat, latent heat, and momentum were computed using standard micrometeorological methods with a rotated, resampled coordinate system from the sensors using eddy covariance, sampled at 20 Hz (Prueger et al., 2000).

The location of the lidar is superimposed on the aerial photographs of the Bosque and Iowa sites (Fig. 1). At the Bosque site, the lidar was situated approximately at the midpoint between the two towers on the western edge of the riparian zone at the top of an adjacent 5-m-high levee (Fig. 1a). At the Iowa site, the lidar was positioned on a fence line between the corn and soybean fields (Fig. 1b).

DISCUSSION

To compute the ILS from lidar data, 78 range-height scans acquired from two experiments (Bosque 1998 and 1999) comprised of five separate days (Bosque 1998 had three and Bosque 1999 had two) representing a wide range of unstable conditions were processed using standard lidar analysis techniques (Eichinger et al., 1999, 2000). The resulting models for L and u_* from the Bosque experiments were then applied to the maturing corn and young soybean agricultural surfaces at SMEX for independent evaluation against eddy-covariance-derived fluxes.

Range-height scans were displayed and prepared for further analysis by extracting horizontal slices parallel to the surface at the tower instrument height, creating a spatial series 300 m long composed of several lines of sight averaged together. Using several methods to evaluate the spatial source area, Cooper et al. (2003) found that several 300-m-long transects acquired during a 15- to 30-min period were an adequate spatial sample for surface layer studies. This analysis suggests that the assumption of trading space for time is reasonable. Typically, one or two range-height data files were averaged together for further processing. In the Bosque case, the analysis involves relatively short time periods for comparisons between the lidar-derived products and tower-based values of L . Thus, the comparisons for the individual values are primarily for verification of the ILS to L relationship. For the SMEX case, however, multiple range-height scans for each azimuth scan angle were averaged together during a 30-min period to create a statistically significant data set for the computation of L , u_* , and LE.

The lidar spatial series were processed using the data conditioning methods described above to estimate Λ from Eq. [6]. Then, values of L were computed from the lidar-derived Λ values using Eq. [16], and u_* was estimated from Eq. [21]. Coincident with the lidar data, tower-based three-axis sonic anemometers, operated at 20 Hz, were also used to measure L and u_* . At SMEX, LE was also derived from the tower measurements with the addition of a fast-response hygrometer and averaged into 30-min values. Finally, the lidar-derived fluxes using both the tower-based micrometeorologically integrated data and the lidar alone were evaluated against the measurements made by the tower-based eddy covariance sensors.

Autocorrelation in Time and Space

An example of coincident autocorrelation functions from the north tower krypton hygrometer and the lidar are shown in Fig. 3. The data shown were acquired on 12 Sept. 1998 between 1440 and 1444 h, during an unstable period with light winds. The time series was 240 s long from the krypton hygrometer, while the spatial series from the lidar required approximately 43 s to acquire (Table 1). Since the scanning period for the lidar is not instantaneous, there is spatial aliasing in the range-height scans due to the time required to capture the data; however, Kao et al. (2002) demonstrated that, under unstable conditions, the scanning period of the lidar is short enough to observe the essential spatial and temporal properties of the vertical eddy structures. They showed this by using a three-dimensional turbulence resolving model that simulates both the atmospheric transport behavior and the lidar scanning patterns used for observing the microscale structures.

In theory, if Taylor's frozen turbulence hypothesis (Tennekes and Lumley, 1972) is valid for the coincident observations acquired, then the lidar-based spatial analysis and the tower-based time-series analysis should be similar. Therefore, we would expect the integral scales from both techniques to be within the expected measurement uncertainty of the instrumentation, on the order of $\pm 10\%$. To test this hypothesis, the sample coincident data sets from the lidar and tower observations shown in Fig. 3 were evaluated in greater detail. The time-series-derived autocorrelation function showed an ξ_{ρ_0} of approximately 25 s (Fig. 3A) and an integral time scale of 7.8 s. By multiplying the integral time scale by the mean wind of 1.2 m s^{-1} , the ILS is 9.4 m. The lidar-derived spatial autocorrelation function dropped zero at an ξ_{ρ_0} of about 20 m (Fig. 3B) and integrated to an ILS of 9.8 m. Dividing the ILS by the mean wind speed produced an integral time scale estimate of 8.1 s (Table 2). Finally, the lidar-derived L calculated from Eq. [16] yielded an estimate of -14.2 m , which is within the measurement uncertainty of the eddy covariance estimate of -15.4 m . The results from coincident time, spatial-series, and similarity solutions yielded L values, integral lengths, and time scales within ± 10 to 15% and were thus within the expected measurement uncertainty, supporting the application of the lidar-based autocorrelation technique to L estimation.

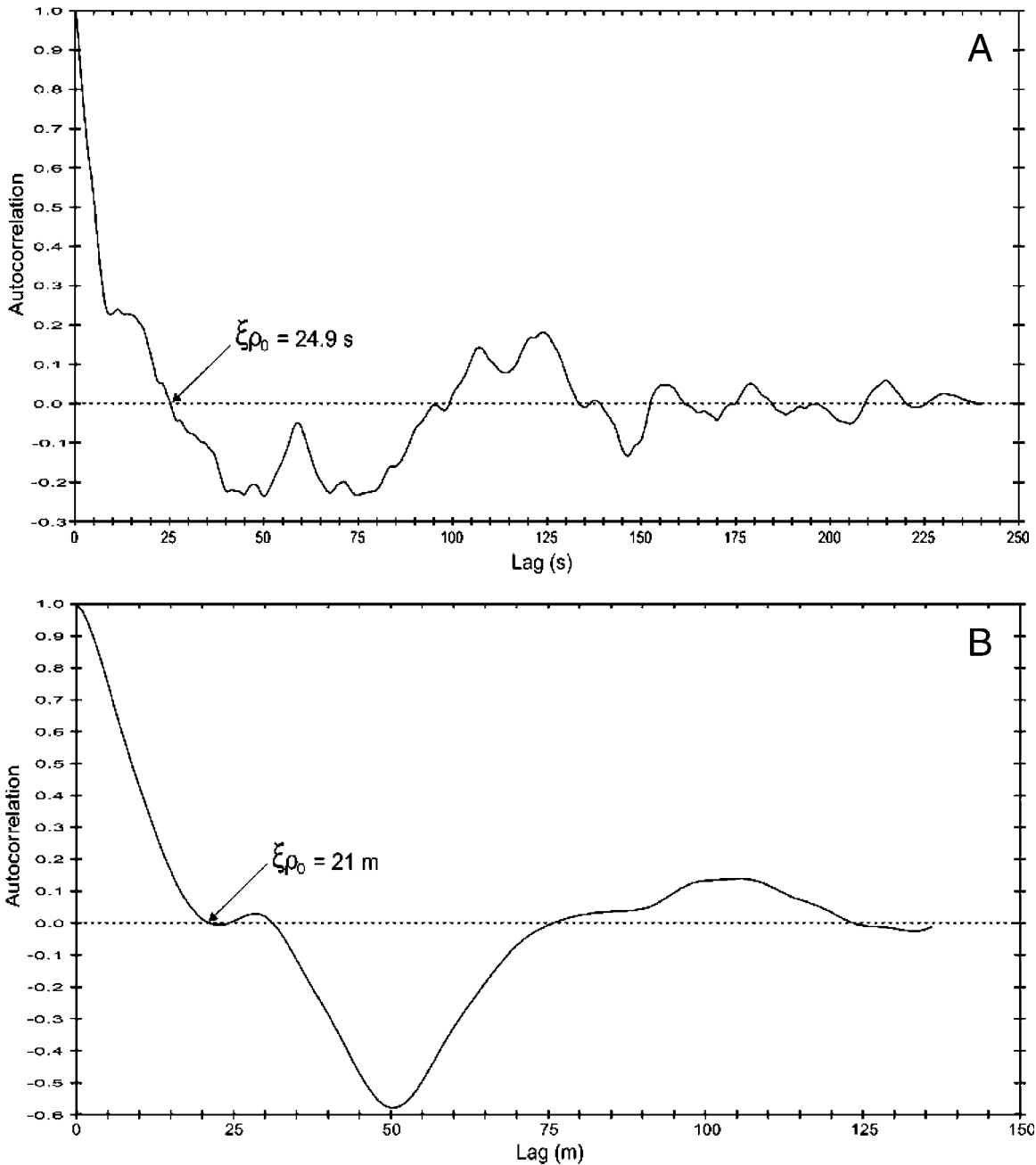


Fig. 3. Comparison of coincident autocorrelation functions from (A) the tower-mounted krypton hygrometer and (B) lidar on 12 Sept. 1998 at 1440 h. The plots show the zero-crossing lag (ξ_{ρ_0}) for each function and their corresponding integral scales.

Taylor’s frozen turbulence theory (Tennekes and Lumley, 1972) is also invoked to interpret the autocorrelation functions. The autocorrelation functions are not weighted for wind direction, thus the implicit assumption is that the turbulent field is isotropic, and surface–atmosphere eddy

circulation is “spherical.” The spherical assumption is dependent on the variations in wind direction within a 30-min averaging period; wide variations will be closer to spherical, while a persistent wind direction will limit its utility. Weighting algorithms for the autocorrelation functions based on the alignment between the lidar scanning azimuth and the prevailing wind direction will be developed in future work to account for the eddy structure.

Table 2. Characteristic scales from the krypton hygrometer and lidar; L is the Obukhov length, τ is the integral time scale, and Λ is the integral spatial scale.

Plot	Source	Start time	Duration	L (tower)		τ	Λ
				s	m		
Fig. 3A	tower	1440 h	240	-15.4	-	7.8	9.4
Fig. 3B	lidar	1444 h	43	-	-14.2	8.1	9.8

Relationship between the Integral Length Scale and the Obukhov Length

To characterize the relationship between lidar ILS and tower-based L estimates across a wide range of un-

stable conditions with the analysis described above, data sets from the Bosque experiments were used, spanning a range of L values between -1 and -200 m. A scatter plot (Fig. 4) shows that, for the unstable case (when $L < 0$), the lidar-derived ILS can be related to L with some confidence. A model curve from Eq. [16] parameterized for the Bosque site is also shown in the figure as a dotted line with $\pm 10\%$ limits on either side. The 10% confidence limits were chosen as the expected uncertainty in estimating L from a sonic anemometer, and linearly propagated into Eq. [16]. The L values are randomly distributed about the $\pm 10\%$ uncertainty bracket. The lidar-derived L scatter plot follows the expected decaying power-law curve (Squires and Eaton, 1991). The uncertainty in the ILS to L relationship appears relatively constant at ± 10 to 15% except at the smallest L values between 0 and -30 m. The minimum lidar-derived ILS value of 3 m is due to the limited spatial resolution of the lidar of 1.5 m, and the spatial Nyquist frequency is 3 m. When Λ is < 6 , the model appears to overestimate L by upward of 50% .

Least squares regression analysis was used to statistically evaluate the quality of the lidar-derived estimates using Eq. [16] and the eddy covariance measurements of L . A scatter plot of eddy covariance L vs. lidar-derived

values is shown in Fig. 4A. The least-squares regression statistics between the lidar and the eddy-covariance-measured L values resulted in a linear regression model $y = 0.89x - 5.75$ with an r^2 of 0.64 and a standard error of ± 36 m (Fig. 4A). The lidar-derived L values generally underestimated the eddy-covariance-measured L by approximately 10 to 30% for L values between -30 and -200 m. The data from Fig. 4A also suggest that for conditions when L is less than -100 , the uncertainty is large.

Friction Velocity Estimates from Lidar

The L values derived from Eq. [16] were used as input to the u_* model. The comparison of the lidar-estimated u_* with coincident values measured by a three-axis sonic anemometer are shown in Fig. 5. The regression equation for the comparison is $1.01x - 9.3 \times 10^{-4}$ and an r^2 of 0.65 . The modest coefficient of determination is understandable since the errors and uncertainties in the L model propagate directly into the u_* model. Even with this important limitation, the u_* model is useful in supporting spatially resolved flux estimation from the lidar until a better technique is developed. Thus, with the Obukhov length model (Eq. [16]) and the friction velocity model (Eq. [21]), it is now possible to estimate the latent energy flux from

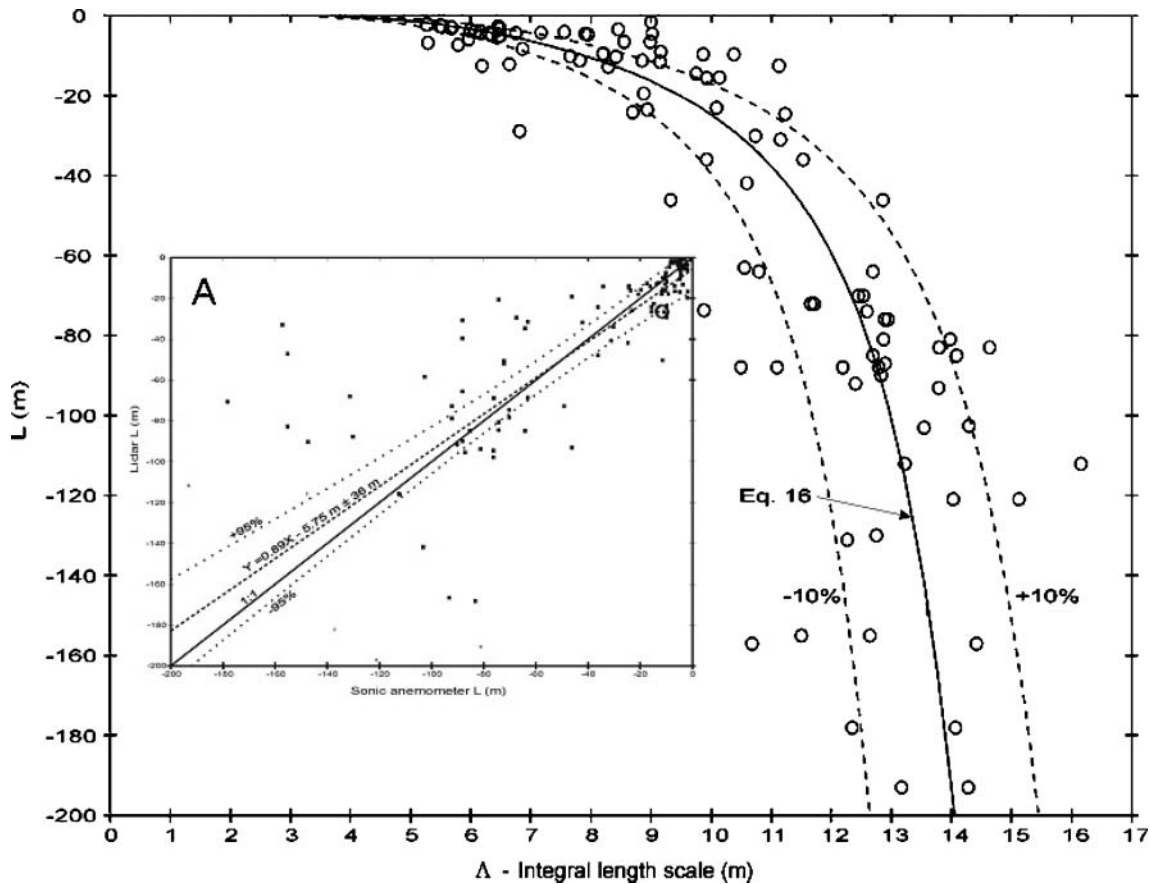


Fig. 4. Relationship between lidar and eddy covariance derived integral spatial scales and the Obukhov length estimated from the Bosque experiments. The similarity model based on a stability function is shown as a dotted line and the $\pm 10\%$ uncertainty functions are shown as dashed lines. Inset A shows statistical analysis of eddy covariance sonic anemometer measured Obukhov length (L) versus lidar-derived values (points), where the solid line is the unity scale and the least-squares regression line (dotted line with equation) is shown with $\pm 95\%$ confidence intervals.

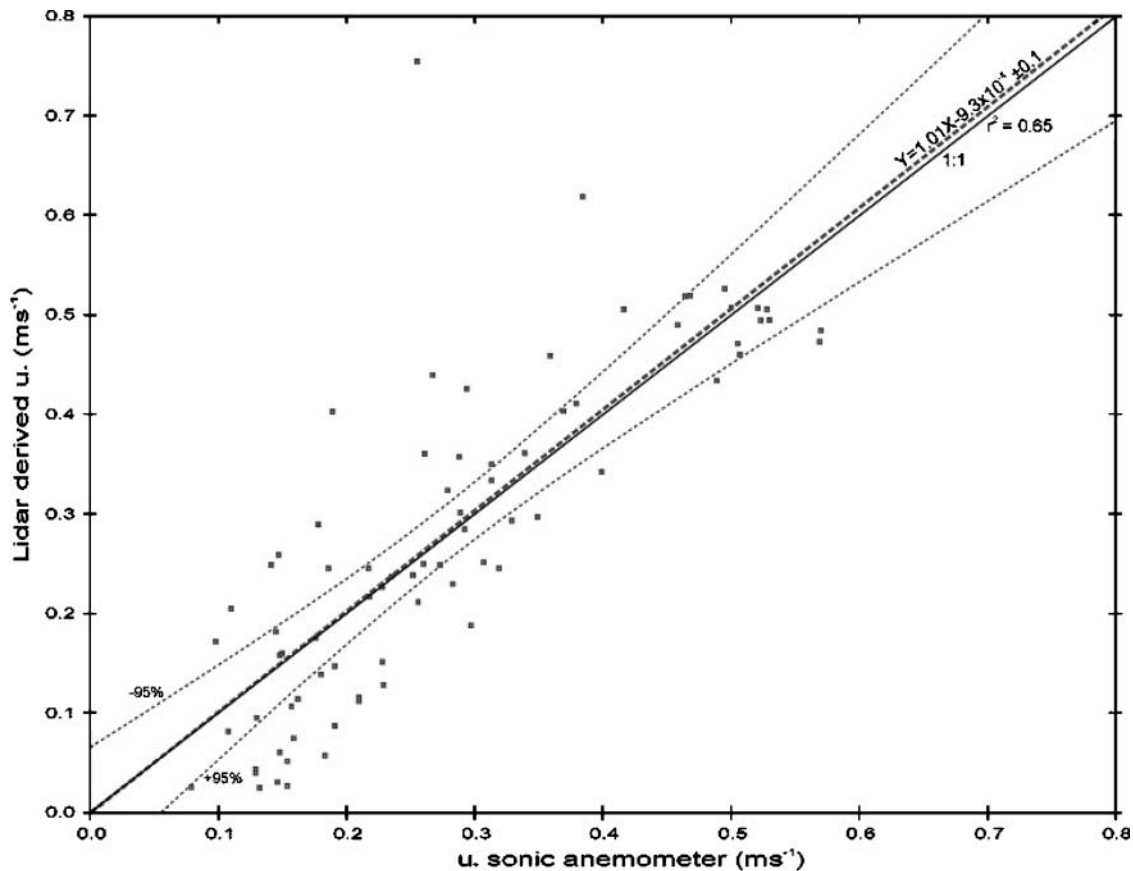


Fig. 5. Scatter plot showing the relationship between sonic anemometer measured and lidar-estimated friction velocity (u_*). The dashed line is the least-squares regression fit, and the solid line is the 1:1 line. The dotted lines are the 95% confidence intervals for the regression line.

lidar data with no additional external measurements under convective conditions.

Comparison of Latent Energy Flux Techniques

During the SMEX experiment, the lidar was programmed to collect range-height scans every 10° in azimuth continuously. This operation resulted in a rich data set for estimating the latent energy flux using the method described in Eichinger et al. (2000, 2006), and Eq. [2] (called here the micrometeorological integrated similarity approach or MISA). Further, an advanced method using the models shown in Eq. [16] and [21] was used in place of the tower-based measurements of L and u_* to estimate the flux without any other observations but the lidar (called here the integral scale similarity approach, ISSA). Histograms of the lidar-derived flux distribution from the two methods were generated and compared with the eddy-covariance fluxes. The eddy-covariance latent energy fluxes were corrected for the basic micrometeorological corrections outlined in Lee et al. (2004) (called simply LE) and further adjusted for closure correction using the Twine et al. (2000) technique (called LE_{CC}). Briefly, the Twine et al. (2000) closure correction assumes the following: that the energy budget should be closed, that eddy covariance always underestimates the fluxes, and that the magni-

tude of the underestimation of sensible heat and latent energy fluxes are partitioned via the Bowen ratio. It is thought by the community at large that the actual (true) latent energy flux resides between the unadjusted and closure-corrected values. A comparison of flux maps derived from lidar data using the ISSA method and the older MISA is shown in Fig. 6. Also shown in the figure are histograms of the lidar-derived flux distributions from the corn and soybean fields, as well as the eddy covariance flux values of LE and LE_{CC} superimposed on the histograms.

The two lidar LE maps show similar spatial properties, with the high flux patterns somewhat oriented with the mean wind. The most obvious difference between the two maps is that the ISSA method shows higher soybean fluxes. The histograms over the corn from the MISA and ISSA are roughly the same and the majority of the distribution is contained within the eddy covariance observations. In contrast, the soybean flux distributions support the use of the ISSA over the MISA, as the MISA appears to underestimate the eddy covariance measurements. Perhaps the open canopy environment of the soybean leads to greater L or u_* uncertainty, suggesting that more study is warranted. Since the flux maps derived from the two analysis techniques appear, in general, to be similar in structure, the primary MISA assumption of uniform L and u_* values for subkilometer ranges is supported, although

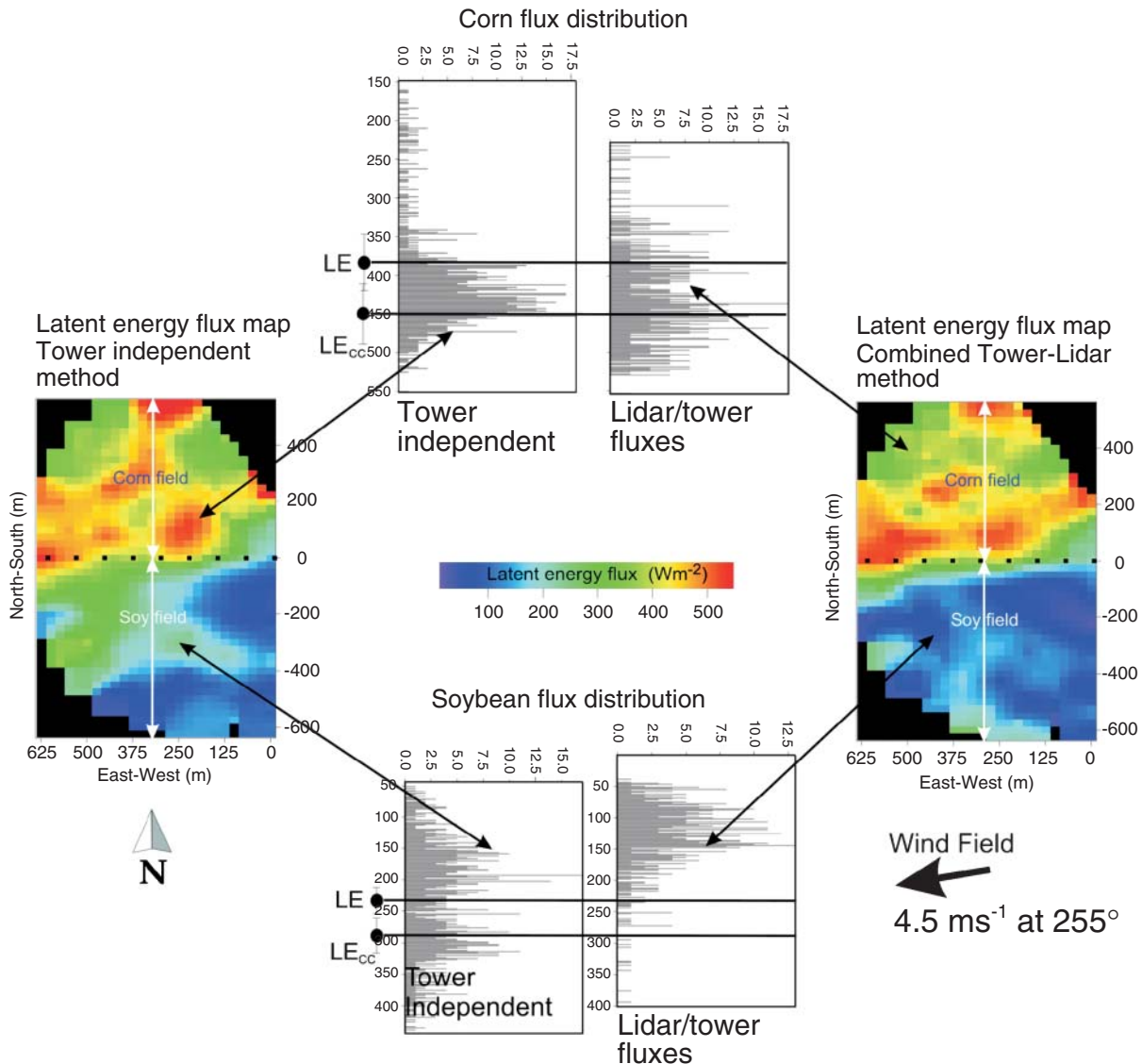


Fig. 6. Comparison of latent energy flux maps derived by tower-independent method (integral scale similarity approach, ISSA) and tower-lidar method (micrometeorological integrated similarity approach, MISA) compiled from data acquired at the Soil Moisture Experiment on 1 July 2002 at 1045 h. The dotted lines on the flux maps show the location of the fence line separating the corn from the soybean. Also shown in the figure are histograms of the spatial distribution of the fluxes from the corn and soybean flux maps, and the latent energy (LE) flux measured by eddy covariance instruments mounted on 3-m towers in the corn and soybean fields. The two eddy covariance points on each histogram refer to the LE flux and the closure-corrected flux (LE_{cc}). The uncertainty bars on the eddy covariance measurements are $\pm 10\%$.

the ISSA appears to be an improvement over MISA within the uncertainty limits of existing similarity theory.

CONCLUSIONS

The Obukhov length, L , is a characteristic measure of the effects of stability on energy and mass transfer in the lower ABL. Traditional methods for estimating L uses three-axis sonic anemometers to measure the time-dependent eddy covariance of wind components and virtual temperature. One of the goals for the scanning Raman lidar is to map fluxes. The present technique, however, requires point sensors, such as sonic anemometers, to support the lidar methodology. We have shown experimentally that L and u_* can be estimated with spatially resolved water vapor observations acquired by

the scanning Raman lidar by a purely statistical property of the data. The autocorrelation of lidar-measured water vapor is used to compute the ILS, which is subsequently scaled to L values using an appropriate similarity relationship. From the analysis of the micrometeorological data across the separate experiments with differing species and plant-soil-water conditions, the lidar-derived ILSs are distributed randomly about the Obukhov length model across a wide variety of unstable conditions from $L < -30$ to $L < -200$. At L values between 0 and -30 , the uncertainty is higher, due in part to the lidar spatial Nyquist frequency of at least 3 m, which propagates into the model as uncertainty in estimating small L values.

The comparisons between the flux maps and the eddy covariance data over agronomic surfaces suggest that the ability to spatially resolve turbulence parameters

such as the Obukhov length and the friction velocity, along with the gradients of water vapor, has a positive effect on the quality of lidar-derived fluxes, even with the higher levels of uncertainty associated with the models. While the resulting LE flux differences between the MISA and ISSA methods aren't dramatic, it is clear that a method independent of external flux sensors is preferred. Direct comparison between L values from the lidar ISSA method and eddy covariance measurements indicates that the methods presented leave room for improvement. Either the eddy covariance data is correct and the limits to the similarity framework for the lidar approach have not been reached, or the variability observed in both the time and spatial series expresses the actual properties of the turbulent fields. If this is the case, then substantial improvements beyond what is presented here will be limited until a better understanding of turbulent exchange is developed. Even with the higher uncertainty at low L values, the relationship between the ILS and L is valid, useful, and powerful. This work brings the concept of independent remotely sensed fluxes much closer to reality with Obukhov length and friction velocity estimates derived from the autocorrelation function of spatial-series data. Future work will evaluate the effect of wind direction on the autocorrelation functions. In addition, we will characterize how well this technique operates with other types of lidars (i.e., elastic-backscatter aerosol systems) since, in theory, the behavior of any passive scalar will be similar to water vapor in an unstable atmosphere. Further, this relationship should be tested over other surfaces and extended to stable conditions.

APPENDIX: LIST OF SYMBOLS

c_p is the specific heat of air ($\text{J kg}^{-1} \text{K}^{-1}$)
 C_1 is the height adjusted profile fitting constant
 d is the displacement height (m)
 g is the acceleration due to gravity (m s^{-2})
 h is the height of the canopy above ground (m)
 k is the von Karman constant
 K is the eddy diffusivity ($\text{m}^2 \text{s}^{-1}$)
 l_e is the latent heat of vaporization (J kg^{-1})
 L is the Obukhov length (m)
 LE is the latent energy flux (W m^{-2})
 q_s is the water vapor mixing ratio at the surface (kg kg^{-1})
 $q(z)$ is the water vapor mixing ratio at height z (kg kg^{-1})
 u_* is the friction velocity (m s^{-2})
 u is the downwind component (m s^{-1})
 v is the crosswind component (m s^{-1})
 w is the vertical wind component (m s^{-1})
 σ_w^2 is the variance in the vertical wind ($\text{m}^2 \text{s}^{-2}$)
 z_0 is the surface roughness (m)
 $w'\theta_v'$ is the time-averaged virtual sensible heat flux ($\text{J m}^{-2} \text{s}^{-1}$)
 β is a profile fitting constant
 Λ is the integral length scale (m)
 θ_v is the virtual temperature (K)
 ξ is the lag in space or time (m or s)
 ξ_{po} is the first zero crossing of the autocorrelation function (m or s)
 ρ is the air density (kg m^{-3})
 τ is the integral time scale (s)
 ϕ_w is the profile function for momentum
 ψ_v is the stability correction function for water vapor

ACKNOWLEDGMENTS

We would like to thank A. Fernandez of LANL, Martha Anderson and William Kustas of USDA-ARS for their technical insights, and Steve Hansen and Steve Bowser of the Bureau of Reclamation for their support. This work was performed and funded in part under DOE Grant W7405-ENG-36.

REFERENCES

- Baldocchi, D. 1997. Flux footprints within and over forest canopies. *Boundary-Layer Meteorol.* 85:273–292.
- Blackadar, A.K. 1997. *Turbulence and diffusion in the atmosphere*. Springer, New York.
- Brutsaert, W. 1982. *Evaporation into the atmosphere. Theory, history, and applications*. Reidel Publ. Co., Dordrecht, the Netherlands.
- Campbell Scientific. 1998. CSAT3 three dimensional sonic anemometer instruction manual. Campbell Scientific, Logan, UT.
- Cooper, D., W. Eichinger, D. Holtkamp, R. Karl, Jr., C. Quick, W. Dugas, and L. Hipps. 1992. Spatial variability of water vapor turbulent transfer within the boundary layer. *Boundary-Layer Meteorol.* 61:389–405.
- Cooper, D.I., W.E. Eichinger, J. Archuleta, L. Hipps, J. Kao, M.Y. Leclerc, C.M. Neale, and J. Prueger. 2003. Spatial source-area analysis of three dimensional moisture fields from lidar, eddy covariance, and a footprint model. *Agric. For. Meteorol.* 114:213–234.
- Cooper, D.I., W.E. Eichinger, S. Barr, W. Cottingham, M.V. Hynes, C.F. Keller, C.F. Lebeda, and D.A. Poling. 1996. High resolution properties of the equatorial pacific marine atmospheric boundary layer from lidar and radiosonde observations. *J. Atmos. Sci.* 53: 2054–2075.
- Cooper, D.I., W.E. Eichinger, L. Hipps, J. Kao, J. Reisner, S. Smith, S.M. Schaeffer, and D.G. Williams. 2000. Spatial and temporal properties of water vapor and flux over a riparian canopy. *Agric. For. Meteorol.* 105:161–183.
- Durand, P., F. Thoumieux, and D. Lambert. 2000. Turbulent length-scales in the marine atmospheric mixed layer. *Q. J. R. Meteorol. Soc.* 126:1889–1912.
- Eichinger, W., D.I. Cooper, F. Archuleta, D. Hof, D. Holtkamp, R. Karl, Jr., C. Quick, and J. Tiee. 1994. Development and application of a scanning, solar-blind water Raman-lidar. *Appl. Opt.* 33: 3923–3932.
- Eichinger, W.E., D.I. Cooper, L.C. Chen, L. Hipps, and C.Y.J. Kao. 2000. Estimation of spatially distributed latent heat flux over complex terrain from a Raman lidar. *Agric. For. Meteorol.* 105:238–261.
- Eichinger, W.E., D.I. Cooper, P.R. Forman, J. Griegos, M.A. Osborn, D. Richter, L.L. Tellier, and R. Thornton. 1999. The development of Raman water-vapor and elastic aerosol lidars for the central equatorial Pacific experiment. *J. Oceanic Atmos. Technol.* 16: 1753–1766.
- Eichinger, W.E., D.I. Cooper, L.E. Hipps, W.P. Kustas, C.M.U. Neale, and J.H. Prueger. 2006. Spatial and temporal variation in evapotranspiration using Raman lidar. *Adv. Water Resour.* 29:369–381.
- Frisch, U. 1995. *Turbulence*. Cambridge Univ. Press, Cambridge, UK.
- Garratt, J.R. 1992. *The atmospheric boundary layer*. Cambridge Univ. Press, Cambridge, UK.
- Kaimal, J.C., and J.J. Finnigan. 1994. *Atmospheric boundary layer flows*. Oxford Univ. Press, New York.
- Kao, C.-Y.J., D.I. Cooper, J.M. Reisner, W.E. Eichinger, and M. Ghil. 2002. Probing atmospheric turbulence with high-resolution lidar and models. *J. Geophys. Res.* 107(D10):4081, doi:10.1029/2001JD000746.
- Kustas, W.P., T.J. Jackson, J.H. Prueger, J.L. Hatfield, and M.C. Anderson. 2003. Remote sensing field experiments evaluate retrieval algorithms and land-atmosphere modeling. *EOS Trans. Am. Geophys. Union* 84(45):485–493.
- Lee, X., W. Massman, and B. Law (ed.). 2004. *Handbook of micrometeorology: A guide for surface flux measurement and analysis*. Atmosph. Oceanogr. Sci. Libr. 29. Kluwer Academic Publ., London.
- Lenschow, D.H., and B.B. Stankov. 1986. Length scales in the convective boundary layer. *J. Atmos. Sci.* 43:1198–1209.
- Mahrt, L. 1998. Flux sampling errors for aircraft and towers. *J. Atmos. Ocean Technol.* 15:416–429.
- Merry, M., and H.A. Panofsky. 1976. Statistics of vertical motion over land and water. *Q. J. R. Meteorol. Soc.* 102:255–260.

- Monin, A.S., and A.M. Yaglom. 1971. *Statistical fluid mechanics*. Cambridge Univ. Press, Cambridge, UK.
- Pope, S.B. 1998. *Turbulent flows*. Cambridge Univ. Press, Cambridge, UK.
- Panofsky, H.A., and J.A. Dutton. 1984. *Atmospheric turbulence models and methods for engineering applications*. Wiley Interscience, New York.
- Panofsky, H.A., H. Tennekes, D.H. Lenschow, and J.C. Wyngaard. 1977. The characteristics of turbulent velocity components in the surface layer under convective conditions. *Bound-Layer Meteorol.* 11:355-361.
- Press, W.H., B.P. Flannery, S.A. Teukolsky, and W.T. Vetterling. 1989. *Numerical recipes*. 2nd ed. Cambridge Univ. Press, Cambridge, UK.
- Prueger, J.H., L.E. Hipps, J.L. Hatfield, and W.P. Kustas. 2000. Turbulence characteristics in a dense riparian tamarisk canopy. p. 204-205. *In Proc. Conf. Agric. and For. Meteorol.*, 24th, Davis, CA. 14-18 Aug. 2000. Am. Meteorol. Soc., Boston, MA.
- Raupach, M.R. 1989. Applying Lagrangian fluid mechanics to infer scalar source distributions from concentration profiles in plant canopies. *Agric. For. Meteorol.* 47:85-108.
- Squires, K.D., and J.K. Eaton. 1991. Lagrangian and Eulerian statistics obtained from direct numerical simulations of homogeneous turbulence. *Phys. Fluids A* 3:130-143.
- Stull, R. 1988. *An introduction to boundary layer meteorology*. Kluwer Acad. Publ., Boston, MA.
- Tennekes, H., and J.L. Lumley. 1972. *A first course in turbulence*. MIT Press, Cambridge, MA.
- Twine, T.E., W.P. Kustas, J.M. Norman, D.R. Cook, P.R. Houser, T.P. Meyers, J.H. Prueger, P.J. Starks, and M.L. Wesely. 2000. Correcting eddy-covariance underestimates over a grassland. *Agric. For. Meteorol.* 103:279-300.
- Wilson, J.D., G.W. Thurtell, and G.E. Kidd. 1981. Numerical simulation of particle trajectories in inhomogeneous turbulence: III. Comparison of predictions with experimental data for the atmospheric surface layer. *Boundary-Layer Meteorol.* 21:443-463.